Toroidal plasma acceleration due to NBI fast ion losses in LTX-β

P.E. Hughes,[1, a)] W. Capecchi,[2] D.B. Elliott,[3] L.E. Zakharov,[4] R.E. Bell,[1] C. Hansen,[5] D.P. Boyle,[1] S.N. Gorelenkov,[1] R. Majeski,[1] and R. Kaita[1]

[1)] *Princeton Plasma Physics Laboratory, Princeton, NJ, USA*
[2)] *University of Wisconsin, Madison, WI, USA*
[3)] *Oak Ridge National Laboratory, Oak Ridge, TN, USA*
[4)] *Lithium Wall Fusion, NJ, USA*
[5)] *University of Washington, Seattle, WA, USA*

(Dated: 28 May 2021)

The recent Lithum Tokamak Experiement–Beta (LTX-β) upgrade includes the addition of neutral beam injection (NBI) in the same direction as the plasma current (co-I_P) and a new toroidal Mirnov array for MHD characterization. In initial NBI experiments, a spontaneously rotating $n = 1$ MHD mode is seen to accelerate during NBI in the counter-beam direction, accompanied by a rise in electron density consistent with the beam-injected inventory but without a clear increase in plasma pressure. Together with analytic and numerical modeling of beam optics and fast ion confinement, these observations indicate the prompt loss of all or nearly all beam ions. However, the same modeling also suggests that planned upgrades to the Ohmic heating system should provide the fast ion confinement necessary for beam heating and core fueling. A simple analytic model relates the momentum confinement time τ_ϕ to the observed evolution of mode rotation due to the combination of NBI momentum coupling, fast ion loss $\vec{J} \times \vec{B}$, and anomalous viscous torques, yielding τ_ϕ values consistent with past measurements of electron energy confinement time $\tau_{E,e}$.

I. INTRODUCTION

It has been known for some time that a lithium plasma-facing surface can retain hydrogen isotopes, creating a "low-recycling" condition[1] without a cold "wind" of recycled neutral gas.[2] Without edge cooling, the plasma is thermally decoupled from the wall, permitting the edge temperature to approach the core temperature.[2] The resulting flat temperature gradients eliminate thermal conduction, and energy losses become limited by particle diffusion.[3] This new confinement regime has the potential to dramatically simplify multiple physics and engineering challenges in fusion energy development.[4,5]

The observation in the Lithium Tokamak Experiment (LTX) of such a regime with flat electron temperature T_e and increased electron energy confinement time, indicating low recycling,[6,7] has motivated the LTX-β upgrade. Cold edge fueling being incompatible with low recycling, LTX exhibited a transient state in which electron density n_e decayed as the flat T_e regime developed. This need for hot core fueling has been addressed with the addition of a neutral beam,[7,8] the application of which to spherical tokamaks has been well studied in various machines.[9,10] The introduction of well-coupled NBI would also permit studies of low recycling discharges with strong auxiliary heating. Maintaining high n_e improves the precision of profile measurements from Thomson scattering, and the addition of the neutral beam provides access to impurity ion temperature T_i^{Li} profiles through CHERS.[8]

The LTX-β upgrade has also compelled the installation of new magnetic diagnostics, including a toroidal Mirnov array of poloidal field sensors in order to study the MHD stability features of the flat T_e regime, especially important as well-coupled neutral beam injection increases plasma pressure β[11] and may interact with existing MHD activity.[12] Additionally, the toroidal field B_{TF} has been increased to 3 kG at $R_0 \approx 35$ cm to improve confinement. A greater B_{TF} impacts the new fast ion population generated by neutral beam injection by reducing gyroradius, although this is not always seen to be a dominant effect,[10] and sustaining a safety factor conducive to MHD stability while increasing accessible I_P to nearly 100kA, leading to tighter drift orbits.[9]

Implementation of the toroidal array in LTX-β permits the use of MHD mode rotation dynamics as a proxy for bulk toroidal plasma acceleration by NBI. Toroidal rotation can be important for MHD mode stabilization, as well as turbulent radial transport suppression by sheared flow.[13,14] Intrinsic rotation arising from transport and electromagnetic effects can be accelerated by neutral beam injection, providing direct momentum deposition in the direction of the beam. Contrastingly, in the presence of fast ion losses, the thermal ion return current[15] $\vec{J}_r$ provides an additional $\vec{J}_r \times \vec{B}$ force whose toroidal component always points in the counter-I_P direction, regardless of NBI orientation.[16]

Remaining sections address engineering, experimental observations, and modeling. Following a characterization of the NBI system, observed differences between beam-injected and baseline LTX-β discharges are discussed, indicating prompt losses and low direct momentum transfer. Analytic and numerical modeling, including an analytic torque balance model, shine-through calculations from TRANSP with NUBEAM,[17] and the 3dOrb code developed by L.E. Zakharov and S.N. Gorelenkov for full-3D fast ion orbit modeling, is employed to develop a physics understanding of the effect of NBI in

[a)] Electronic mail: phughes@pppl.gov

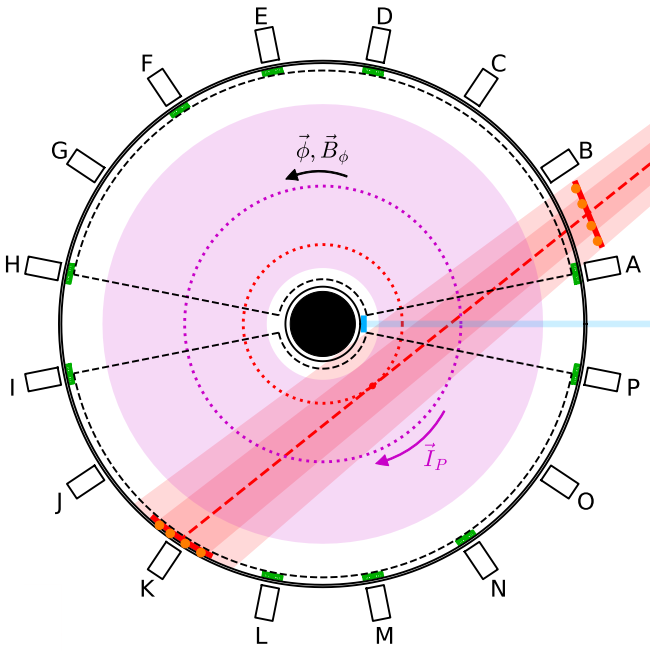

FIG. 1. Geometry of the LTX-β neutral beam and relevant diagnostics in relation to a typical NBI plasma. The neutral beam (shaded red) injects at section AB, crosses a tangency radius of $\approx$ 21 cm (dotted red), and strikes the far side of the vessel (solid black) near toroidal field magnet K. Molybdenum alloy (TZM) scrapers and beam dump (solid red) are instrumented with resistance temperature detector thermal sensors (orange circles). The beam crosses the microwave interferometry sight line (shaded blue) at section PA in the gap between conformal shells (dashed black). Typical plasma major radius (dotted magenta) $R_0 \approx 37$ cm, and reconstructed[19] last-closed flux surface (shaded magenta) includes the beam tangency radius. Toroidal Mirnov array sensors (green) are located between the shells and the vessel wall within the midplane gap between upper and lower shells.

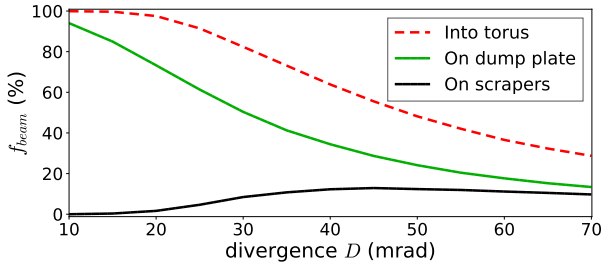

FIG. 2. Fractional power deposition as a function of beam half-angle divergence defined as a Gaussian $1/e$ radius, generated by tracing Gaussian-divergent rays from a point-focused surface-source. Each energy component has a different divergence and fractional power deposition.

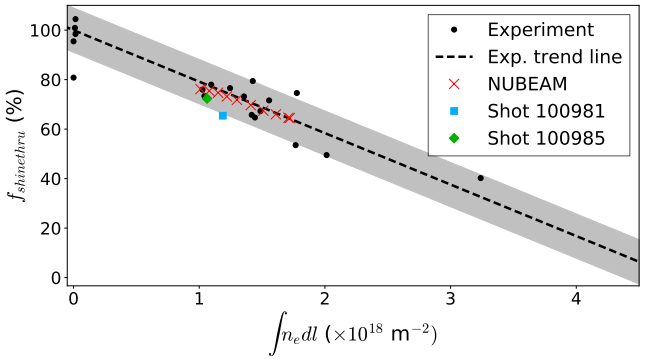

FIG. 3. NBI shinethrough from beam dump calorimetry as a function of line-integrated electron density $\int n_e dl$, comparing experimental data to NUBEAM predictions. Although absolute energy deposited on the beam dump W_{dump} does not match predictions well, the fractional reduction of vacuum W_{dump} remains a good measure of $f_{shinethru}$. The LTX-β full orbit code 3dOrb agrees closely with the NUBEAM shinethrough results.

LTX-β plasmas. This modeling leverages the measured rotation evolution of MHD modes as a telltale of beam performance and to provide insight into the momentum confinement time, typically deduced from spectroscopic measurements.[18] Finally, future steps to improve discharge and NBI performance are laid out.

II. BEAM CHARACTERISTICS AND PERFORMANCE

The neutral beam, oriented for co-I_P injection (Fig. 1), is a Budker Institute of Nuclear Physics device rated for beam energy $E_{NBI} = 20$ keV and beam current $I_{NBI} = 35$ A, which yields a source flux $\Gamma^{src}_{NBI} = 2.2 \times 10^{20}$ s^{-1}, and specified as having a 20 mrad half-angle divergence. The primary diagnostics for neutral beam power injection are calorimetry arrays on the dump plate and scrapers.[8] Assuming nominal operation at the rated 20 mrad divergence and accounting only for the full energy component ($\approx$ 80% of the total power, with 15% and 5% in the half- and third-energy respectively), about 95% of the total beam power should enter the vessel, and the dump plate should absorb roughly half of the total power (Fig. 2). The balance would strike the plasma-facing side of the conformal shells and inner face of the vacuum vessel, with a small fraction reaching the back of the pump duct between magnets J and K (Fig. 1).

The first phase of beam operation was injection into the torus without a target plasma, to characterize beam performance as a function of acceleration grid voltage and current. Expected beam power injection into the torus and deposition on the dump plate and beam scrapers was modeled based on an empirical estimate of $\approx$ 60% illumination by ions of the beam source grid (Fig. 2). One of the main findings was that fractional energy deposited on the beam dump W_{dump}/W_{beam} was significantly less than initially predicted. Rather than the beam dump receiving $\geq$70% of total beam energy W_{beam} as predicted for the manufacturer-specified beam optics, the largest W_{dump}/W_{beam} observed was $\approx$ 13%. Al-

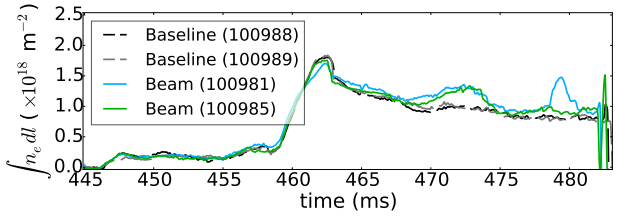

FIG. 4. Line-integrated electron density rises during beam injection (shaded green) on NBI discharges (blue and green), but returns to baseline (black and gray) within about 1 ms.

though this indicated a very high divergence ≈ 70 mrad, the ratio of beam dump energy to beam scraper energy $W_{dump}/W_{scrapers} \approx 2$, suggesting a divergence nearer 50 mrad. Spectroscopic measurements, however, yielded a still lower divergence ≈ 35 mrad, indicating an injection ratio into the vessel $f_{inj} \approx 73\%$, and indicated significantly nonuniform source grid illumination. Because of variations in beam voltage and current throughout beam injection, the beam's perveance and therefore divergence varied, changing power deposition throughout the beam injection period.[8]

Modeling and equipment specifications indicate a theoretical maximum neutralization fraction $f_{neut} \sim 90\%$ in the beam injector, shine-through $f_{shinethru} \sim 70\%$ for the full energy component as predicted by NUBEAM and matched closely by modeling based on typical plasma parameters and preliminary beam characterization experiments (Fig. 3), estimated full-energy f_{inj} from spectroscopy, and reduced injection of the half- and third-energy beam components. Accounting for these parameters, total deposited fraction of source flux

$$f_{dep} \equiv \sum_{\epsilon}^{max} (1 - f^{\epsilon}_{neut})(1 - f^{\epsilon}_{inj})(1 - f^{\epsilon}_{shinethru}) \qquad (1)$$

can be calculated, where $\sum_{\epsilon}$ signifies a sum over beam energy components. $f_{dep} \approx 0.15$. As noted, beam performance varied during injection,[8] but the NBI window average parameters of $E_{NBI} \approx 18$ keV and $I_{NBI} \approx 36$ A were within roughly 10% of their manufacturer-specified values. With these parameters, the beam should supply roughly 100 kW of heating and an optimal (i.e. lossless) fueling rate $\Gamma^{opt}_{NBI} \approx 3.3 \times 10^{19}$ s^{-1} neglecting lost ions. This particle flux represents a total injection of $N_{NBI} \approx 1.8 \times 10^{17}$ hydrogen atoms during a typical 5.5 ms beam pulse. By comparison, the target discharge style studied exhibited a total hydrogen inventory of $N_e \approx 5 \times 10^{17}$ electrons and peak Ohmic heating power $P_{OH} \approx 110$ kW. These estimates indicate a rise in total density of $\approx 30\%$, and an approximate doubling of plasma heating, implying at least a doubling of plasma pressure.

In the discharges studied here, the line-integrated density from microwave interferometry $\bar{n_e} \equiv \int n_e dl$ was seen to increase by $\approx 33\%$, close to the prediction. To ensure

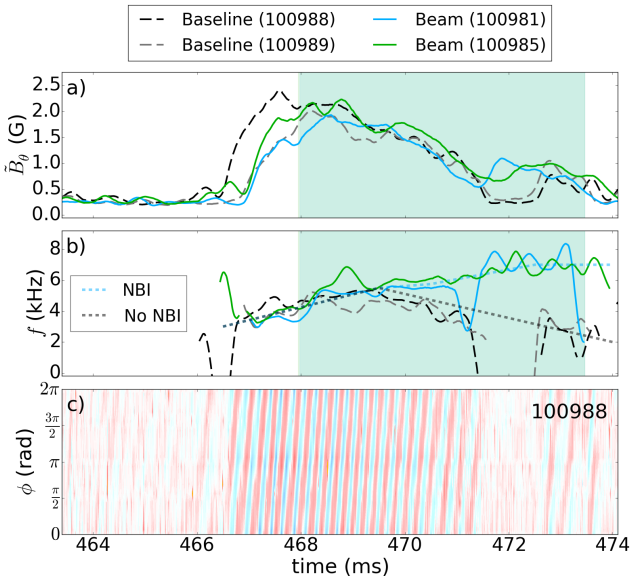

FIG. 5. During the NBI period (shaded green) there is little effect on $n = 1$ MHD mode amplitude (a), but rotation frequency f is accelerated in the $+\phi$ (counter-I_P) direction (b). In plot (b), trend lines indicating the evolution of beam (dotted blue) and non-beam (dotted black) discharges. Plot (c) shows perturbed poloidal field $\tilde{B}_\theta$ measured on the toroidal array as a function of toroidal angle ϕ and time. The phase angle of the $n = 1$ structure (red stripe) is seen to evolve in time, indicating a rotating perturbation. Note that near 472 ms in shot 100988, mode amplitude drops below the threshold for faithful phase tracking.

that the density increase was caused by beam injection, LTX-β discharges were produced with 1. beam not triggered, 2. full beam injection into plasma, 3. beam gas without grid energization, and 4. beam injection blocked by the NBI source's internal calorimetry plate.[8] Only full beam injection produced the observed increase in electron density. Fast camera images showed ~mm scale transient hot spots on the beam dump and wall during injection, but no evidence of significantly elevated surface localized emission. However, drift orbit modeling suggests that lost beam ions may preferentially impact outside the fast camera's line of sight.

It should be noted that the rise in density ended abruptly with the end of the beam discharge and decayed back down to non-beam discharge density in less than 1 ms (Fig. 4). Since the slowing-down time of fast hydrogen ions

$$\tau_s = 6.28 \times 10^8 \frac{T_e^{3/2}}{n_e ln\Lambda} \qquad (2)$$

is expected to be ~ 10 ms,[20] the decay timescale of density to a value similar to that of non-NBI discharges after the end of injection is consistent with the prompt loss of beam ions driving the rapid ambipolar expulsion of excess electrons (discussed in Sec. IV).

III. COMPARISON OF MHD ROTATION TO NBI MOMENTUM TRANSFER TORQUE

Both beam and non-beam discharges characteristically developed $n = 1$ mode activity at about $t = 467$ ms (whereas beam injection begins at $t_{NBI} = 468$ ms), rising to $\approx$ 2 G and decaying to the background by $t \approx 475$ ms (Fig. 5a). This mode appeared to spontaneously rotate in the $+\phi$ direction, which is counter-I_P. In the limiting case of confinement and momentum coupling of co-I_P beam-injected ions and neglecting $\vec{J}_r \times \vec{B}$ forces described in Sec. IV, the observed rotation would be expected to slow and even reverse during beam injection.

Although there was no evidence of any effect of beam injection on mode amplitude, it can be seen in Fig. 5b that the evolution of mode rotation was strongly beam-dependent. In the characteristic non-beam discharge, mode rotation reduced from $\approx$ 5 kHz at 469 ms by $\approx$ 0.5 kHz/ms until the amplitude fell too low for accurate phase tracking (Fig. 5c). In the beam-injected discharges, mode rotation *increased* by $\approx$ 0.3 kHz/ms over the same window.

In addition to fueling and heating of the LTX-β plasma, well-confined beam ions should apply a momentum transfer torque in the co-I_P ($-\phi$, clockwise in Fig. 1) direction. Treating the beam simply as a single central ray with a well-defined tangency radius R_{tan}, the torque from each energy fraction species ϵ with fueling rate Γ_ϵ is

$$\vec{\tau}_{NBI,\epsilon} = \int \Gamma_\epsilon cos(\theta_{dep}) \bar{f}_{dep} \frac{m_p n_e(l)}{\int n_e(l) dl} \vec{R}(l) \times \vec{v_\epsilon} dl, \quad (3)$$

where $\theta_{dep} \equiv \phi(l) + \pi/2$ is the local angle between the ray and the toroidal tangent, $\bar{f}_{dep} \equiv (1 - f_{shinethru})(1 - f_{loss})$ is the expected total ionization fraction along the ray, and the ray velocity is $\vec{v_\epsilon} \equiv (2E_\epsilon/m_p)^{1/2} \vec{e_\epsilon}$.

The geometric terms conveniently cancel, since $R(l) \equiv R_{tan}/sin(\phi(l))$ and $\phi(l) = tan^{-1}(R_{tan}/l)$, leaving $n_e(l)/\int n_e(l) dl$ the only remaining l-dependent term. This cancels as well once integrated, reducing Eq. 3 to

$$\vec{\tau}^{ray}_{NBI} = m_p \sum_\epsilon \Gamma_\epsilon f_{dep} \vec{R}_{tan} \times \vec{v_\epsilon}. \quad (4)$$

The beam's finite divergence is accounted for by summing over many rays η,

$$\vec{\tau}_{NBI} = m_p \sum_\eta \sum_\epsilon \Gamma^\eta_\epsilon \bar{f}^\eta_{dep} \vec{R}^\eta_{tan} \times \vec{v_\epsilon}, \quad (5)$$

where each ray is assigned a specific ray flux Γ^η_ϵ based on a parabolic beam intensity profile, tangency radius R^η_{tan}, and mean ionized fraction $\bar{f}^\eta_{dep}$ (normalized by the ratio of $\int n_e dl$ for ray η to $\int n_e dl$ of the central ray).

The toroidal-plane moment of inertia for a toroid of arbitrary cross-section is

$$I_{tor} = \int_R \int_Z 2\pi R^3 m_p n_e(Z, R) dZ dR, \quad (6)$$

where the shape and profile information are carried in $n_e(Z, R)$. Using typical LTX-β elongation $\kappa = 1.5$, triangularity $\delta = 0.2$, major radius $R_0 \approx 0.37$ m, minor radius $a \approx 0.22$ m, and $\int n_e dl \approx 1.0 \times 10^{18}$ m^{-2} with a Wesson-like[21] n_e profile ($n_e = n_0(1 - (r/a)^2)^{\nu_J}$) where n_0 is the on-axis density and $\nu_J = 2$ is the Wesson parameter, $I_{tor} \approx 1.0 \times 10^{-10}$ kg m^2.

Taking the observed 35 mrad divergence but neglecting fast ion losses, $\vec{\tau}_{NBI} \sim -18\hat{z}$ mN-m with $\hat{z}$ the vertical unit vector. However, because momentum deposits on the relatively long slowing-down timescale τ_s (Eq. 2), the total increase in mode rotation predicted during beam injection is $\Delta f_{MHD} \approx -3.5$ kHz, which would reverse the direction of toroidal rotation in the case of no fast ion losses and $\tau_s \approx 8$ ms.

Since mode acceleration was observed in the $+\phi$ direction, which is counter-I_P and counter-beam, the dominant torque during beam injection was clearly not beam momentum transfer. Recovering the observed rotation evolution requires properly accounting for the $\vec{J}_r \times \vec{B}$ torque due to prompt fast ion losses and viscous damping.

IV. MODELING OF TORQUES DUE TO LOST FAST IONS

Understanding the discrepancies between optimal (i.e. lossless) and observed effects of neutral beam injection on LTX-β discharges requires faithful tracking of the distribution of beam deposition, momentum and energy transfer, and fast ion loss. The 3dOrb particle tracking code uses the LSODE solver[22] to calculate coordinates and velocities of charged particles due to the Lorentz force in a tokamak magnetic field. Trajectories are tracked until intersection with machine geometry to provide surface deposition profiles. In NBI simulations, the initial conditions for fast ions are generated by random charge exchange events along the beam trajectory within the plasma. 3dOrb and TRANSP with NUBEAM have both indicated that given observed beam optics and plasma parameters consistent with the beam-injection run campaign (i.e. $I_P \sim 75$ kA), practically all full-energy fast ions are prompt losses. Although some half-energy ($\sim 27\%$) and third-energy ($\sim 43\%$) fast ions are retained, these represent only 5% of the total expected torque deposition. Modeling of electrostatic confinement in 3dOrb (Fig. 6) indicates that finite potential effects can be neglected in modeling ion loss for these discharges.

Typical LTX-β discharges of interest exhibited an uncommonly broad low-field side (LFS) scrape-off layer (SOL) based on PSI-Tri equilibrium reconstructions[19],

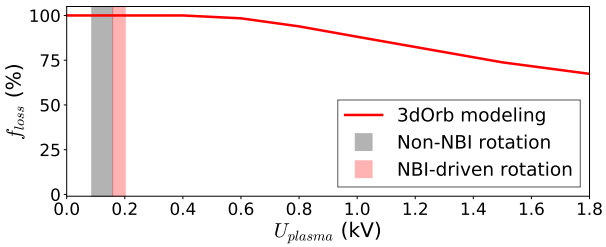

FIG. 6. Prompt loss fraction of 18keV fast ions as a function of plasma potential U_{plasma} calculated by 3dOrb. Estimating $U_{plasma} \approx v_{\vec{E}\times\vec{B}} B_\theta a$, shaded regions represent the potential estimated from taking slow (non-NBI) and fast (NBI-accelerated) toroidal rotation velocities as $\vec{v}_{\vec{E}\times\vec{B}}$.

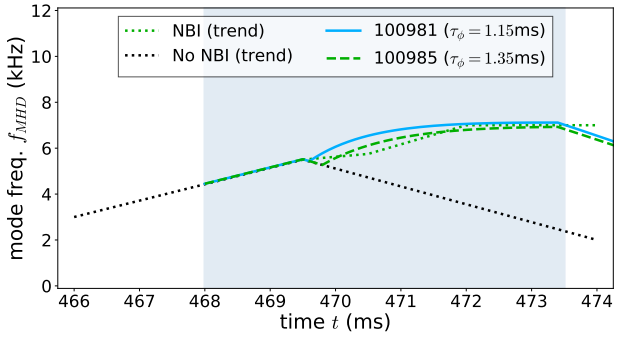

FIG. 7. Mode rotation evolution scenarios assuming full fast ion prompt loss f_{loss}, per 3dOrb modeling. All other beam and plasma parameters are typical of the discharge identified. The momentum transport timescale τ_ϕ is used as a free parameter to fit to observed rotation evolution.

as well as very large beam ion orbits. In LTX-β, $\rho_{fi}/a \approx 0.28$ near the magnetic axis and was even greater near the LFS edge, where ρ_{fi} is the fast ion gyroradius and a is plasma minor radius. Given that ρ_{fi}/a was so large, certain assumptions made by TRANSP may be violated, as seen in other spherical tokamaks[9,23], suggesting that a full orbit code such as 3dOrb should be more reliable for non-collisional modeling of fast ions in LTX-β. Because prompt loss occurs on a time scale much shorter than the fast ion collision time, it can be assumed that single particle drift orbit geometry is the dominant factor in fast ion losses.

The above tracking of fast ion losses is key to understanding the observed acceleration of modes in the $+\phi$ (counter-beam) direction. Given a total beam current of 36A, assuming 24A (67% per Fig. 2) enters the torus, approximately 7A ($\sim 30\%$ per Fig. 3) of that total is reionized by charge exchange within the plasma volume. Because this fast ion population's collisional damping to the bulk population is weak ($\nu \propto v^{-3}$ for particles with $v > v_{th}$, with $v_{fi} \gg v_{th}$), the effective radial current of fast ions being lost confers a $\vec{J}\times\vec{B}$ torque only on the retained co-I_P fast ion population. However, the resulting electric field drives a polarization drift preferentially transporting thermal ions inward to replace the lost fast ions, which in the presence of significant momentum transport, produces a return current[15] that couples its $\vec{J}\times\vec{B}$ torque strongly to the bulk plasma.[24,25]

The torque due to the $\vec{J}_r \times \vec{B}$ force acts in both the toroidal and poloidal directions, driving both toroidal and poloidal flow. Since toroidal and poloidal mode rotation look identical on a toroidal array and the poloidal mode number m is not well-characterized in LTX-β, the evolution of mode rotation can only be interpreted faithfully in scenarios in which the poloidal flow is strongly damped on timescales much shorter than the beam injection period.

The dominant mechanism of poloidal flow damping depends on the ratio of ion collisional timescale τ_{ii} to the poloidal ion flow timescale $q_a R_0/v_{th,i}$ where q_a is edge safety factor and $v_{th,i}$ is the ion thermal velocity. In LTX-β, estimating T_i from spectroscopy measurements of $T_i^{Li} \approx 25$ eV, this ratio is close to unity, suggesting that magnetic pumping is driven by a combination of parallel thermal conductivity (rotation-dominated diffusion) and parallel viscosity (collision-dominated diffusion). The poloidal flow damping timescale τ_d for these mechanisms were $\tau_d^{cond} \sim \tau_{ii} \approx 90$ μs and $\tau_d^{visc} \sim (q_a R_0 m_i/T_i)^2/\tau_{ii} \approx 20$ μs, respectively,[26] for the discharges of interest. Since the poloidal flow damping mechanism timescales were more than an order of magnitude shorter than the beam injection period, it is safe to say that any poloidal flow was saturated during beam injection, so all changes in rotation can be assumed to have been toroidal,[27,28] and the toroidal component of Eq. 7 can be expressed using only $\vec{B}_\theta$.

Representing the fast ion loss generated torque in a simplified form,

$$\vec{\tau}_{\vec{J}\times\vec{B}} \approx \langle \vec{R} \times (\vec{J}_r \times \vec{B}) V_{\vec{J}} \rangle, \tag{7}$$

where $V_{\vec{J}}$ is the weighted mean volume through which the radial current passes, estimated as $V_{\vec{J}} \approx V_{plasma}(1 - r_{dep}^2/r_a^2)$ with r_{dep} the weighted mean minor radius of charge deposition.

Assuming the prompt (i.e. before any momentum or transferred to the bulk plasma) loss of all fast ions consistent with 3dOrb modeling, the resulting $\vec{\tau}_{\vec{J}\times\vec{B}}$ from Eq. 7 is roughly 5 mN-m. The toroidal $\vec{J}\times\vec{B}$ torque is complicated, however, by the generation of an anomalous viscous torque which acts as a drag on toroidal rotation, evolving on a toroidal momentum transport timescale τ_ϕ.[27] We can estimate this anomalous torque as

$$\vec{\tau}_{anom} \approx m_p \langle n_e V_{\vec{J}} \rangle \vec{R} \times \vec{v}_\phi / \tau_\phi, \tag{8}$$

where $\langle n_e V_{\vec{J}} \rangle$ is particle inventory averaged over $V_{\vec{J}}$. The resulting angular acceleration gradually damps down as $\vec{\tau}_{anom}$ increases with the $\vec{J}\times\vec{B}$-driven velocity, consistent with the behavior expected of a viscous drag term.

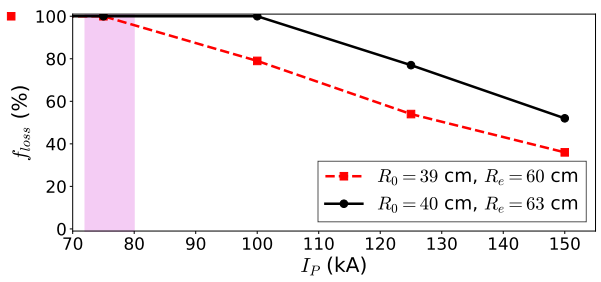

FIG. 8. Fast ion prompt loss predictions to increased I_P, calculated in 3dOrb with 18keV ions and plasma major radius at $R_0 = 39$ cm (dashed red) and $R_0 = 40$ cm (solid black). Both cases limit on the high-field side at $R_{HFS} = 14$ cm. Plasma geometry including magnetic axis and edge radii plays a significant role in fast ion confinement due to the importance of beam neutral charge-exchange profile and the large gyroradius of beam ions in LTX-β. Full or near-full prompt loss is predicted in the range of plasma currents observed during beam injection (shaded magenta).

The summation of torques is performed by tracking the time-resolved deposition of beam ions, distributing their momentum transfer torque over the slowing-down time τ_s (Eq. 2). For simplicity, ions are regarded as being either well-confined or prompt losses, without accounting for effects such as pitch angle scattering. To reflect the finite momentum transport timescale, $\vec{\tau}_{\vec{J}\times\vec{B}}$ and $\vec{\tau}_{anom}$ are only added starting from $t = t^{trig}_{NBI} + t^{on}_{NBI} + \tau_\phi$ where $t^{trig}_{NBI} = 468$ ms is the time of NBI initiation and $t^{on}_{NBI} \approx 0.5$ ms is the rise-time of I_{NBI}. Empirically, this delay is intended also to reflect the observed delay between NBI initiation and the deviation of rotation in NBI discharges relative to non-NBI discharges.

Using the same radial transport volume estimate $V_{\vec{J}}$ employed to calculate $\vec{\tau}_{\vec{J}\times\vec{B}}$, and taking the toroidal momentum transport term as a free parameter, we find that $\tau_\phi \approx 1.25$ ms reproduces the observed rotation evolution from Fig. 5b well (Fig. 7) given the full prompt loss scenario predicted by 3dOrb (Fig. 8). Empirical observations support the intuitive assumption that the magnitude of τ_ϕ is typically similar to $\tau_{E,i}$.[16,18,27] Given the estimates of $\tau_{E,e} \sim 1$ ms previously observed in LTX-β,[6] this further supports the full prompt ion loss scenario.

V. SUMMARY AND FUTURE WORK

The LTX-β upgrade's emphasis on the use of neutral beam injection to sustain density and increase heating without dependency on cold edge fueling necessitates a thorough physics understanding of the beam-plasma interaction. Although the increase in electron density is consistent with specified performance, there was no evidence of a change in pressure based on diamagnetic measurements and MHD stability (Fig. 5a).

The observed acceleration of magnetic perturbations in the direction opposite the (co-I_P) beam injection is consistent with the prompt loss of all or nearly all fast ions so that the radial current driven $\vec{J}_r \times \vec{B}_\theta$ torque dominates completely over angular momentum deposition torque. This provides an alternative means of estimating the momentum confinement time via MHD rotation evolution, rather than the time evolution of plasma rotation profiles from spectroscopy.[18] Likewise, easily-automated MHD rotation analysis can in certain discharge styles serve as a coarse experimental indicator of beam ion confinement.

The implementation of the 3dOrb code has allowed for calcuation of prompt fast ion losses, key to understanding NBI driven torque. This is known to require faithful orbit tracking in spherical tokamaks due to potential non-conservation of the magnetic moment,[10,23] as well as a consistent treatment of radial electric field accumulation.[15,29] Commonly, fast ion loss is due to excursions by particles that would have well-confined gyrocenters in a guiding center model.[9] However, 3dOrb calculations show that the primary prompt loss mechanism of LTX-β beam ions is strong vertical drift, with about 20% depositing on the low-field side. Ongoing work explores details of full orbit modeling and plasma geometry effects in LTX-β relevant scenarios.

In order to improve beam performance, the beam gas supply valves have recently been upgraded, and plans are underway to increase the stored energy capacity of the power supplies. Preventing the beam current from drooping will increase control of the beam perveance, which influences divergence. Further power supply upgrades are planned to extend the beam extraction period from 5 ms to $\geq$15 ms, increasing the window of beam fueling.

To improve fast ion confinement, plans are underway to double the stored energy of the Ohmic heating capacitor bank, increasing peak accessible plasma current. 3dOrb calculations indicate that increasing I_P to 125 kA (an increase of 67% from the discharge style described here) may decrease prompt fast ion losses from near 100% to $\sim$40% by improving fast ion orbits[9] if the plasma is kept strongly high-field side limited (Fig. 8). This difference in prompt loss fraction should be clearly detectable in the total applied toroidal acceleration, and in a clear difference in heating.

Since LTX-β discharges have achieved line-integrated mean density $\bar{n}_e \sim 7.5 \times 10^{18}$ m^{-2}, empirical observations (Fig. 3) also imply that full deposition and reduced slowing-down times should be accessible with moderate changes to discharge style. Increased density and heating will also improve CHERS light, providing a spectroscopic measurement of ion rotation profiles.

Once LTX-β is able to clearly demonstrate good confinement of fast ions, it will be possible to explore the evolution of density and pressure during neutral beam injection as a function of fast ion losses. Studying this relationship between n_e, β_p, and f_{loss} will allow testing of the above hypothesis for the lost beam ion driven density increase, and more importantly, a less transient low-recycling regime with NBI heating and core fueling.

ACKNOWLEDGMENTS

This work was supported by U.S. DOE contract numbers DE-AC02-09CH11466, DE-AC05-00OR22725, and DE-SC0019239. Special thanks to Timothy Stoltzfus-Dueck for insights into momentum transport, Shigeyuki Kubota for implementation and maintenance of the microwave interferometry system, Filippo Scotti for operation and analysis of fast cameras, and to the LTX project technical staff.

[1] M. Baldwin, R. Doerner, S. Luckhardt, and R. Conn, Nuclear Fusion **42**, 1318 (2002).
[2] S. I. Krasheninnikov, L. E. Zakharov, and G. V. Pereverzev, Physics of Plasmas **10**, 1678 (2003).
[3] L. E. Zakharov, VANT **34**, 29 (2011).
[4] L. E. Zakharov, Nuclear Fusion **59**, 096008 (2019).
[5] L. E. Zakharov, J. P. Allain, S. Bennett, M. Abdelghany, and D. Bulgadaryan, (2020).
[6] D. P. Boyle, R. Majeski, J. C. Schmitt, C. Hansen, R. Kaita, S. Kubota, M. Lucia, and T. D. Rognlien, Phys. Rev. Lett. **119**, 015001 (2017).
[7] R. Majeski *et al.*, Physics of Plasmas **24**, 056110 (2017).
[8] D. Elliott *et al.*, IEEE Trans. Plas. Phys. **8**, 1382 (2020).
[9] R. Akers, L. Appel, P. Carolan, N. Conway, G. Counsell, M.Cox, S. Gee, M. Gryaznevich, R. Martin, A. Morris, M. Nightingale, A. Sykes, M. Mironov, and M. Walsh, Nuclear Fusion **42**, 122 (2002).
[10] W. Heidbrink, M. Miah, D. Darrow, B. LeBlanc, S. Medley, A. Roquemore, and F. Cecil, Nuclear Fusion **43**, 883 (2003).
[11] P. E. Hughes, R. Majeski, R. Kaita, T. Kozub, C. Hansen, and D. P. Boyle, Review of Scientific Instruments **89**, 10J104 (2018).
[12] W. Heidbrink, E. Ruskov, D. Liu, L. Stagner, E. Fredrickson, M. Podestà, and A. Bortolon, Nuclear Fusion **56**, 056005 (2016).
[13] A. M. Garofalo, E. J. Strait, L. C. Johnson, R. J. La Haye, E. A. Lazarus, G. A. Navratil, M. Okabayashi, J. T. Scoville, T. S. Taylor, and A. D. Turnbull, Phys. Rev. Lett. **89**, 235001 (2002).
[14] G. Staebler, R. Waltz, and J. Wiley, Nuclear Fusion **37**, 287 (1997).
[15] K. G. McClements and A. Thyagaraja, Physics of Plasmas **13**, 042503 (2006).
[16] J. Rice, Journal of Physics: Conference Series **123** (2008), 10.1088/1742-6596/123/1/012003.
[17] A. Pankin, D. McCune, R. Andre, G. Bateman, and A. Kritz, Computer Physics Communications **159**, 157 (2004).
[18] S. Suckewer, H. P. Eubank, R. J. Goldston, E. Hinnov, and N. R. Sauthoff, Phys. Rev. Lett. **43**, 207 (1979).
[19] C. Hansen, D. P. Boyle, J. C. Schmitt, and R. Majeski, Physics of Plasmas **24**, 042513 (2017), https://doi.org/10.1063/1.4981214.
[20] T. H. Stix, Plasma Physics **14**, 367 (1972).
[21] J. Wesson, Nuclear Fusion **18**, 87 (1978).
[22] A. C. Hindmarsh, "ODEPACK, a systematized collection of ODE solvers," in *Scientific Computing* (North-Holland, Amsterdam, 1983) pp. 55–64.
[23] M. Cecconello, W. Boeglin, D. Keeling, S. Conroy, I. Klimek, R. Perez, and The MAST team, Nuclear Fusion **59**, 016006 (2019).
[24] J. S. deGrassie, R. J. Groebner, and K. H. Burrell, Physics of Plasmas **13**, 112507 (2006).
[25] Y. Koide *et al.*, Proc. 14th Int. Conf. on Plasma Physics and Controlled Nuclear Fusion Research **1**, 777 (1993).
[26] A. B. Hassam and R. M. Kulsrud, The Physics of Fluids **21**, 2271 (1978), https://aip.scitation.org/doi/pdf/10.1063/1.862166.
[27] C. Chang, Nuclear Fusion **39**, 2113 (1999).
[28] M. Honda *et al.*, Nuclear Fusion **48**, 085003 (2008).
[29] A. Thyagaraja, F. Schwander, and K. G. McClements, Physics of Plasmas **14**, 112504 (2007).